Research Square

Preprints are preliminary reports that have not undergone peer review.
They should not be considered conclusive, used to inform clinical practice,
or referenced by the media as validated information.

Bupivacaine induces cardiotoxicity in human iPSC-derived cardiomyocytes through mitochondrial dysfunction and oxidative stress-associated apoptosis: attenuation by Intralipid

Ting Jiang
Xi'an Children's Hospital
Zhe Zhao
Xi'an Children's Hospital
Wenjun huang
Xi'an Children's Hospital
Min Wang
Xi'an Children's Hospital
Ni Wang
Xi'an Children's Hospital
Wenming Song
Xi'an Children's Hospital
Shuang Zhang
Xi'an Children's Hospital
Yi Miao
my876921190163.com
Xi'an Children's Hospital

Research Article

Keywords: bupivacaine, cardiotoxicity, hiPSC-derived cardiomyocytes, mitochondrial dysfunction, oxidative stress, apoptosis, Intralipid

Posted Date: November 3rd, 2026

DOI: https://doi.org/10.21203/rs.3.rs-11242254/v1

License: This work is licensed under a Creative Commons Attribution 4.0 International License.
Read Full License

Additional Declarations: No competing interests reported.

Abstract

Bupivacaine is a widely used local anesthetic, but its cardiotoxicity during local anesthetic systemic toxicity (LAST) remains incompletely characterized in human-relevant cardiac models. In this study, human induced pluripotent stem cell-derived cardiomyocytes (hiPSC-CMs), generated using the GiWi monolayer differentiation protocol, were exposed to bupivacaine for 24 or 48 hours. Cell viability, cytotoxicity, spontaneous beating activity, mitochondrial function, oxidative stress, and apoptotic signaling were evaluated. Bupivacaine reduced cell viability in a dose- and time-dependent manner, with estimated IC_{50} values of approximately 550 μM at 24 hours and 312 μM at 48 hours, and significantly impaired spontaneous beating rate and rhythm regularity at concentrations ≥ 100 μM. Mechanistically, bupivacaine induced mitochondrial membrane depolarization and mitochondrial fragmentation, accompanied by increased expression of the fission-related proteins DRP1 and FIS1 and decreased expression of the fusion-related proteins MFN2 and OPA1. These changes were associated with increased intracellular reactive oxygen species (ROS), an elevated BAX/BCL2 ratio, increased cytochrome c expression, and enhanced caspase-3 cleavage, indicating activation of the intrinsic mitochondrial apoptotic pathway. Co-treatment with Intralipid significantly restored cell viability, preserved mitochondrial membrane potential, reduced oxidative stress, and attenuated apoptotic signaling in bupivacaine-exposed hiPSC-CMs. These findings suggest that bupivacaine induces cardiotoxicity through a mitochondria–ROS–apoptosis cascade involving dysregulated mitochondrial dynamics, and provide mechanistic cellular evidence supporting Intralipid as a rescue agent for LAST-associated cardiotoxicity.

1 Introduction

Bupivacaine is a long-acting local anesthetic widely used in regional anesthesia, epidural blockade, and perioperative analgesia because of its potent sensory blockade and prolonged duration of action (El-Boghdadly et al. 2018). However, among commonly used local anesthetics, bupivacaine is associated with a relatively high risk of cardiotoxicity, particularly in the setting of local anesthetic systemic toxicity (LAST) caused by inadvertent intravascular injection or excessive systemic absorption (El-Boghdadly and Chin 2016). LAST may present with conduction disturbances, arrhythmias, cardiovascular collapse, and refractory ventricular fibrillation, making bupivacaine-induced cardiac injury an important safety concern in clinical anesthesia practice (Marrone et al. 2026; Neal et al. 2018). Clarifying the cellular mechanisms underlying this toxicity may help improve cardioprotective strategies and refine rescue interventions.

Previous studies have shown that bupivacaine can inhibit cardiac sodium channels, interfere with potassium channel activity, impair mitochondrial respiratory chain function, and induce apoptosis in cardiomyocytes (Sztark et al. 1998; Lu et al. 2011; Haraguchi et al. 2015). In particular, mitochondrial dysfunction has been recognized as a key contributor to bupivacaine-induced cardiac injury, as impaired oxidative phosphorylation and mitochondrial membrane depolarization can promote reactive oxygen species (ROS) accumulation and apoptotic signaling (Sztark et al. 1998; Lu et al. 2011). Nevertheless,

much of the available evidence has been derived from animal cardiomyocytes, isolated heart preparations, or heterologous ion channel expression systems. These models have important translational limitations because they do not fully recapitulate human cardiomyocyte electrophysiology, metabolic characteristics, or integrated contractile behavior (Karakikes et al. 2015).

Human induced pluripotent stem cell-derived cardiomyocytes (hiPSC-CMs) provide a human-relevant platform for evaluating drug-induced cardiotoxicity. They retain key cardiac electrophysiological and contractile features and have been increasingly used for mechanistic cardiotoxicity studies and preclinical safety assessment (Ewoldt et al. 2025). Despite this advantage, the mechanisms of bupivacaine-induced injury in hiPSC-CMs remain insufficiently characterized. In particular, the role of mitochondrial dynamics, including the balance between fusion and fission regulated by MFN1, MFN2, OPA1, DRP1, and FIS1, has not been clearly defined in human cardiomyocytes exposed to bupivacaine. Whether bupivacaine activates intrinsic mitochondrial apoptotic signaling, characterized by cytochrome c involvement and caspase-3 cleavage, also requires further investigation in a human cardiac model.

Intravenous lipid emulsion is recommended as a rescue therapy for LAST-associated cardiovascular toxicity, but the cellular mechanisms underlying its cardioprotective effects remain incompletely understood (Nendumba et al. 2025). Proposed mechanisms include sequestration of lipophilic local anesthetics, improved myocardial energy substrate availability, and attenuation of mitochondrial injury and oxidative stress. However, direct evidence in human cardiomyocytes remains limited.

Therefore, this study aimed to investigate the mitochondrial mechanisms underlying bupivacaine-induced cardiotoxicity in hiPSC-CMs and to determine whether Intralipid attenuates these effects by preserving mitochondrial integrity, reducing oxidative stress, and suppressing intrinsic apoptotic signaling.

2 Methods

2.1 Cell Lines and Culture Conditions

Two human pluripotent stem cell lines were used in this study. Human induced pluripotent stem cells (hiPSCs) and the HN4 human embryonic stem cell (hESC) line (HES-P20-P9) were both purchased from OSINGLAY BIO (China) and maintained under feeder-free conditions. Both cell lines were cultured in BioCISO medium (BC-PM0001, OSINGLAY BIO, China) on Matrigel-coated (354277, Corning, UK) 6-cm plates at 37°C in a humidified atmosphere containing 5% CO_2. The medium was refreshed daily, and cells were passaged every 4–5 days using 0.5 mM EDTA when confluency reached 80–90%. All experiments were performed using both cell lines between passages 20 and 40.

2.2 Isolation of peripheral blood mononuclear cells (PBMCs)

Peripheral blood mononuclear cells (PBMCs) were isolated from healthy donor whole blood by density gradient centrifugation. Briefly, peripheral blood was diluted 1:1 with phosphate-buffered saline (PBS) and carefully layered onto Ficoll-Paque solution (density 1.077 g/ml) in a 15 ml conical tube. After centrifugation at 400 × g for 30 min at room temperature with the brake off, the buffy coat layer containing PBMCs was carefully aspirated and washed twice with PBS at 300 × g for 10 min. The isolated PBMCs were resuspended in RPMI-1640 medium supplemented with 10% fetal bovine serum (FBS) and counted using a hemocytometer. Cells were either used immediately for downstream experiments or cryopreserved in 90% FBS / 10% DMSO at − 80°C until use.

2.3 Differentiation of hiPSCs into cardiomyocytes

Cardiomyocyte differentiation was performed using the GiWi protocol as previously described, with minor modifications (Lian et al. 2013). Briefly, hiPSCs at 80–90% confluency were dissociated with 0.5 mM EDTA and seeded at 0.5 × 10^5 cells/ml onto Matrigel-coated 12-well plates in BioCISO medium supplemented with 10 μM ROCK inhibitor Y-27632 (day − 4). On day 0, the medium was replaced with RPMI 1640 / B-27 (without insulin) containing 10 μM CHIR99021 (S1263, Sigma, USA), a GSK-3 inhibitor, for 24 h to activate Wnt signaling. On day 1, the medium was changed to RPMI 1640 / B-27 (without insulin) and maintained for 48 h. On day 3, the medium was replaced with RPMI 1640 / B-27 (without insulin) containing 5 μM IWP-2 (3533, Tocris Bioscience, UK), a Wnt inhibitor, for 48 h. From day 5 to day 7, cells were maintained in RPMI 1640 / B-27 without insulin. From day 7 onwards, the medium was refreshed every 3 days with RPMI 1640 / B-27 containing insulin. Spontaneous beating was typically observed from day 8.

To enrich the cardiomyocyte population, metabolic purification was performed from day 10 to day 12 by incubating beating monolayers in glucose-free RPMI 1640 supplemented with 4 mM sodium DL-lactate for 48 h, selectively eliminating non-cardiomyocytes while preserving lactate-utilizing cardiomyocytes. Cells were subsequently returned to RPMI 1640 / B-27 containing insulin for at least 48 h recovery. Cardiomyocyte purity, assessed by flow cytometry with anti-cTnT antibody, routinely exceeded 85%.

2.4 Characterization of hiPSCs and hiPSC-derived cardiomyocytes using the Immunofluorescence staining

For characterization of hiPSCs, cells were seeded on Matrigel-coated glass coverslips and fixed with 4% paraformaldehyde (PFA) in PBS for 15 min at room temperature. After washing three times with PBS, cells were permeabilized with 0.3% Triton X-100 in PBS for 10 min and blocked with 5% normal donkey serum (NDS) in PBS for 1 h at room temperature. Cells were then incubated overnight at 4°C with the following primary antibodies: anti-OCT4 (1:100, ab19857, Abcam, UK), anti-SOX2 (1:200, ab97959, Abcam, UK), anti-NANOG (1:100, ab214549, Abcam, UK), and anti-SSEA4 (1:200, ab16287, Abcam, UK). For trilineage differentiation assessment, cells were stained with anti-CXCR4 (1:100, ab124824, Abcam, UK), anti-BRACHYURY (1:200, ab140661, Abcam, UK), anti-AFP (1:400, #35190, CST, USA), anti-SOX17 (1:100, MA5-24885, Invitrogen, USA), anti-PAX6 (1:100, 42-6600, Invitrogen, USA), and anti-NESTIN (1:500, ab18102, Abcam, USA) using the same protocol. After washing, cells were incubated with

appropriate Alexa Fluor-conjugated secondary antibodies (1:500, Invitrogen, USA) for 1 h at room temperature in the dark. Nuclei were counterstained with DAPI (1 μg/ml) for 5 min. Coverslips were mounted with anti-fade mounting medium and imaged using a fluorescence microscope (Olympus, Japan).

For characterization of hiPSC-derived cardiomyocytes (hiPSC-CMs), cells at day 21 and day 35 were fixed and stained as described above using the following primary antibodies: anti-cardiac troponin T (cTNT; 1:200, MA5-12960, Invitrogen, UK), anti-α-actinin (1:200, ab68167, Abcam, UK), anti-Ki67 (1:500, #9129, CST, UK), and anti-NKX2.5 (1:200, PA5-49431, Invitrogen, UK).

Quantitative real-time PCR (qRT-PCR)

Total RNA was extracted from PBMCs, human embryonic stem cells (hESCs), hiPSCs, and hiPSCs derived cardiomyocytes using TRIzol reagent (Thermo Fisher Scientific, USA) according to the manufacturer's instructions. RNA concentration and purity were assessed using a NanoDrop spectrophotometer (Thermo Fisher Scientific, USA). Complementary DNA (cDNA) was synthesized from 1 μg total RNA using a reverse transcription kit (Takara Bio, Japan). Quantitative PCR was performed on a real-time PCR system using SYBR Green Master Mix (Takara Bio, Japan). The expression levels were quantified using the 2^(−ΔΔCt) method and normalized to the housekeeping gene GAPDH. All reactions were performed in triplicate. Primer sequences are listed in Table S1.

Flow cytometry

The purity of hiPSC-CM cultures at day 21 was assessed by flow cytometry. Cells were dissociated with 0.25% trypsin-EDTA, washed with PBS, and fixed with 4% PFA for 15 min at room temperature. After washing, cells were permeabilized with 0.1% saponin in PBS containing 0.5% bovine serum albumin (BSA) for 15 min. Cells were then incubated with anti-cardiac troponin T (cTNT; 1:200, MA5-12960, Invitrogen, UK), or anti-α-actinin (1:200, ab68167, Abcam, UK) for 30 min at room temperature, followed by incubation with the appropriate fluorochrome-conjugated secondary antibody for 20 min in the dark. Isotype-matched antibodies served as negative controls. Data were acquired on a flow cytometer (BD Biosciences, USA) and analyzed using FlowJo software (v10.0, BD Biosciences, USA). A minimum of 10,000 events were recorded per sample.

2.5 Drug preparation

Bupivacaine hydrochloride (BUP; B5274, Sigma-Aldrich, USA) was dissolved in sterile distilled water to prepare a stock solution at a concentration of 100 mM and stored at − 20°C until use. Working solutions at the indicated concentrations (0, 100, 312, and 550 μM) were freshly prepared by serial dilution in RPMI 1640 / B-27 medium immediately before each experiment. The final volume of vehicle (distilled water) did not exceed 0.1% (v/v) in any experimental condition and had no effect on cell viability or beating behavior (data not shown).

For lipid emulsion rescue experiments, a 20% Intralipid emulsion (Fresenius Kabi, Sweden) was diluted to the working concentration in RPMI 1640 / B-27 medium immediately prior to use. Co-treatment groups received BUP and Intralipid simultaneously at the indicated concentrations.

2.6 Cell viability and cytotoxicity assays

Cell viability was assessed using the Cell Counting Kit-8 (CCK-8; Dojindo, Japan) according to the manufacturer's instructions. Briefly, hiPSC-CMs at day 21 were seeded in 96-well plates at a density of 1 × 10^4 cells/well and allowed to stabilize for 24 h prior to drug treatment. Cells were then exposed to BUP at concentrations of 0, 10, 30, 100, 312, 550, and 1000 μM for 24 h or 48 h. At each time point, CCK-8 reagent (10 μl) was added to each well and incubated at 37°C for 2 h. Absorbance was measured at 450 nm using a microplate reader (BioTek, USA). Cell viability was expressed as a percentage relative to the vehicle control group (0 μM BUP), which was set to 100%.

Cytotoxicity was evaluated by measuring lactate dehydrogenase (LDH) release using an LDH Cytotoxicity Assay Kit (Beyotime, China) according to the manufacturer's instructions. Culture supernatants were collected at 24 h and 48 h after BUP treatment and centrifuged at 400 × *g* for 5 min to remove cell debris. LDH activity in the supernatant was measured at 490 nm. The percentage of LDH release was calculated relative to the maximum LDH release control (cells lysed with lysis buffer provided in the kit), which was set to 100%. All assays were performed in five independent replicates (n = 5).

2.7 Spontaneous beating analysis

Spontaneous beating activity of hiPSC-CMs was recorded at day 28 following 24 h exposure to BUP at concentrations of 0, 100, 312, and 550 μM. Bright-field videos were captured at 37°C using a phase-contrast microscope equipped with a temperature-controlled stage (Olympus, Japan) at a frame rate of 25 frames per second (fps) for a minimum of 60 s per field. Three to five fields of view were recorded per well, and a minimum of three wells were analyzed per condition.

Beating rate (beats per minute, bpm), standard deviation (SD) of inter-beat intervals, and coefficient of variation (CV, %) were quantified per field of view and subsequently averaged across all fields within each well to yield a single representative value per well. Three to five fields of view were recorded per well, and a minimum of three wells were analyzed per condition. For each functional parameter — beating rate, SD of inter-beat intervals, and CV (%) — values obtained from individual fields of view within the same well were averaged to yield a single representative value per well. All statistical analyses were therefore performed at the well level, with n = 5 independent wells per condition, to ensure the independence of observations required for one-way ANOVA.

2.8 Mitochondrial function assessment

Mitochondrial membrane potential (ΔΨm) was evaluated using the JC-1 assay kit (Beyotime, China). hiPSC-CMs were incubated with JC-1 working solution (2 μM) at 37°C for 20 min, washed twice with JC-1 buffer, and immediately imaged by fluorescence microscopy. In healthy mitochondria with high ΔΨm, JC-1 forms red-fluorescent J-aggregates (excitation/emission: 585/590 nm); in depolarized

mitochondria, JC-1 remains as green-fluorescent monomers (excitation/emission: 514/529 nm). The ratio of red to green fluorescence intensity was quantified using ImageJ software and used as an index of mitochondrial membrane potential.

Mitochondrial morphology was assessed using MitoTracker Red CMXRos (100 nM; Thermo Fisher Scientific, USA), which was added to live cells for 30 min at 37°C. Images were acquired by fluorescence microscopy and analyzed for mitochondrial network morphology.

Protein expression of mitochondrial dynamics regulators, including the fusion proteins MFN1, MFN2, and OPA1, and the fission protein DRP1, was assessed by Western blot as described in Section 2.10.

2.9 Oxidative stress and apoptosis detection

Intracellular reactive oxygen species (ROS) levels were measured using the fluorescent probe 2',7'-dichlorofluorescein diacetate (DCFH-DA; Beyotime, China). hiPSC-CMs were incubated with 10 μM DCFH-DA in serum-free medium at 37°C for 20 min, washed three times with PBS, and immediately analyzed using a microplate reader (excitation/emission: 488/525 nm). Mean fluorescence intensity (MFI) was quantified and normalized to the vehicle control group.

Apoptosis-related protein expression was assessed by Western blot. The following proteins were examined: cleaved caspase-3, cleaved caspase-9, Bcl-2, and Bax. The Bax/Bcl-2 ratio was calculated as an index of apoptotic propensity. Protein expression levels were normalized to GAPDH and quantified by densitometry as described in Section 2.10.

2.10 Western blot analysis

Cells were lysed in RIPA buffer (Beyotime, China) supplemented with protease and phosphatase inhibitor cocktail (Thermo Fisher Scientific, USA) on ice for 30 min. Lysates were centrifuged at 12,000 × *g* for 15 min at 4°C, and the supernatant was collected. Protein concentration was determined using the BCA Protein Assay Kit (Thermo Fisher Scientific, USA). Equal amounts of protein (20 μg per lane) were separated by 10–12% SDS-PAGE and transferred onto polyvinylidene fluoride (PVDF) membranes (Millipore, USA). Membranes were blocked with 5% non-fat dry milk in Tris-buffered saline containing 0.1% Tween-20 (TBST) for 1 h at room temperature, followed by overnight incubation at 4°C with the following primary antibodies: anti-cleaved caspase-3 (1:1000, ab32042, Abcam, UK), anti-Bcl-2 (1:1000, ab32124, Abcam, UK), anti-Bax (1:1000, ab32503, Abcam, UK), anti-MFN1 (1:1000, #14739, CST, USA), anti-MFN2 (1:1000, #9482, CST, USA), anti-OPA1 (1:1000, #80471, CST, USA), anti-DRP1 (1:1000, #8570, CST, USA), and anti-GAPDH (1:5000, # 2118, CST, USA). After washing with TBST, membranes were incubated with HRP-conjugated secondary antibodies (1:5000, CST, USA) for 1 h at room temperature. Protein bands were visualized using enhanced chemiluminescence (ECL) reagent (Thermo Fisher Scientific, USA) and imaged with a chemiluminescence imaging system (Bio-Rad, USA). Band intensities were quantified by densitometry using ImageJ software and normalized to GAPDH.

2.11 Statistical analysis

All data are presented as mean ± standard deviation (SD). Statistical analyses were performed using GraphPad Prism software (version 9.0, GraphPad Software, USA). Differences among multiple groups were assessed by one-way analysis of variance (ANOVA) followed by Tukey's post hoc test. Comparisons between two groups were performed using the unpaired Student's *t*-test. A *p*-value of less than 0.05 was considered statistically significant. Statistical significance is indicated as follows: **p* < 0.05, ***p* < 0.01, ****p* < 0.001, *****p* < 0.0001. Each experiment was performed at least three times independently unless otherwise stated. The sample size (n) for each experiment is specified in the corresponding figure legend.

3 Results

3.1 Characterization of hiPSCs

To confirm the pluripotent identity of the hiPSCs used in this study, we examined the expression of key pluripotency markers by qRT-PCR and immunofluorescence staining (Fig. 1). qRT-PCR analysis demonstrated that *OCT4*, *SOX2*, *NANOG*, and *KLF4* were markedly upregulated in hiPSCs compared with PBMCs, and were expressed at levels comparable to those observed in hESCs (Fig. 1B). Immunofluorescence staining confirmed robust nuclear expression of OCT4, SOX2, and NANOG, as well as surface expression of SSEA4, in hiPSC colonies (Fig. 1C). Directed trilineage induction revealed expression of mesoderm markers CXCR4 and BRACHYURY, endoderm markers AFP and SOX17, and ectoderm markers PAX6 and NESTIN (Fig. 1D). These results confirm that the hiPSCs used in this study exhibit characteristic pluripotency marker expression and retain trilineage differentiation capacity, providing a validated cell source for subsequent cardiomyocyte differentiation.

3.2 Characterization of hiPSC-derived cardiomyocytes (hiPSC-CMs)

To validate the efficiency and maturation of cardiomyocyte differentiation, hiPSC-CMs were characterized at day 21 and day 35 by immunofluorescence staining and flow cytometry (Fig. 2). At day 21, immunofluorescence staining revealed co-expression of the cardiac-specific marker cTNT with the cardiac progenitor transcription factor NKX2.5, confirming cardiac lineage commitment (Fig. 2A). A subset of cTNT-positive cells also expressed the proliferation marker Ki67, indicating residual proliferative activity at this stage. Flow cytometry analysis at day 21 demonstrated that 90.2% of cells were α-actinin-positive and 94.5% were cTNT-positive, confirming high-purity cardiomyocyte cultures (Fig. 2C). At day 35, immunofluorescence staining of cTNT and α-actinin revealed well-organized sarcomeric striations, indicative of increased structural maturation compared with day 21 (Fig. 2B). These findings demonstrate that the GiWi differentiation protocol reliably generates high-purity hiPSC-CMs with progressive sarcomeric maturation, establishing a robust cardiac model for evaluating bupivacaine-induced cardiotoxicity.

3.3 Bupivacaine induces dose- and time-dependent cytotoxicity and functional impairment in hiPSC-CMs

To evaluate the cardiotoxic effects of bupivacaine (BUP), hiPSC-CMs were exposed to a range of BUP concentrations (0–1000 μM) for 24 h or 48 h, and cell viability, membrane integrity, and spontaneous beating activity were assessed (Fig. 3). CCK-8 assay revealed that BUP reduced cell viability in a dose- and time-dependent manner across the concentration range of 0–1000 μM (Fig. 3A, B). The IC_{50} was 550 μM at 24 h and 312 μM at 48 h. LDH release assay confirmed a corresponding dose-dependent increase in membrane damage at both time points, with significantly elevated LDH levels observed at concentrations ≥ 100 μM compared with the vehicle control (Fig. 3C, D).

Analysis of spontaneous beating activity following 24 h BUP exposure revealed significant functional impairment in a dose-dependent manner (Fig. 3E–G). Beating rate showed a progressive declining trend across the 100, 312, and 550 μM groups, with statistically significant reductions observed at 312 μM and 550 μM compared with the 0 μM control (Fig. 3E). The standard deviation of inter-beat intervals was significantly increased at all three concentrations (100, 312, and 550 μM; Fig. 3F), and the coefficient of variation (CV, %) was similarly elevated across all tested concentrations, indicating that beating irregularity emerged even at the lowest dose examined (Fig. 3G; *p < 0.05, ***p < 0.001, ****p < 0.0001 vs. 0 μM). These data demonstrate that BUP induces dose- and time-dependent cytotoxicity and disrupts spontaneous electromechanical activity in hiPSC-CMs, with 312 μM representing a critical threshold concentration; subsequent mechanistic investigations therefore focused on this concentration.

3.4 Bupivacaine induces mitochondrial membrane depolarization, fragmentation, and dysregulation of mitochondrial dynamics

To investigate the effects of BUP on mitochondrial function and dynamics, hiPSC-CMs were treated with BUP at 0, 312, and 550 μM for 24 h, and mitochondrial membrane potential, morphology, and dynamics-related gene and protein expression were assessed (Fig. 4). JC-1 staining revealed a significant reduction in the J-aggregates/J-monomers fluorescence ratio at both 312 μM and 550 μM compared with the vehicle control, indicating dose-dependent mitochondrial membrane depolarization (Fig. 4A, B; $^{**}p < 0.01$ vs. 0 μM). MitoTracker Red staining demonstrated progressive mitochondrial fragmentation with increasing BUP concentrations, with elongated mitochondrial networks in control cells replaced by punctate, fragmented structures at 312 and 550 μM (Fig. 4C).

At the transcriptional level, treatment with 312 μM BUP significantly downregulated the expression of mitochondrial fusion genes *MFN1*, *MFN2*, and *OPA1*, while upregulating the fission genes *DRP1* and *FIS1* compared with untreated controls (Fig. 4D; $^{*}p < 0.05$ to $^{**}p < 0.01$). Western blot analysis confirmed these findings at the protein level: fusion-related proteins MFN2 and OPA1 were significantly decreased (Fig. 4E; $^{*}p < 0.05$ and $^{***}p < 0.001$, respectively), while fission-related proteins DRP1 and FIS1 were significantly increased following 312 μM BUP treatment (Fig. 4F; $^{*}p < 0.05$ vs. 0 μM). These results

indicate that BUP impairs mitochondrial membrane potential and shifts the mitochondrial fusion–fission balance toward fission, prompting further investigation into whether this mitochondrial dysfunction is accompanied by oxidative stress and activation of apoptotic signaling.

3.5 Bupivacaine induces oxidative stress and activates the mitochondrial apoptotic pathway

To determine whether BUP-induced mitochondrial dysfunction was accompanied by oxidative stress and apoptosis, intracellular ROS levels and apoptosis-related protein expression were examined in hiPSC-CMs treated with BUP for 24 h (Fig. 5). DCFH-DA fluorescence assay revealed a significant dose-dependent increase in intracellular ROS levels at 312 μM and 550 μM BUP compared with the vehicle control (Fig. 5A; $^{**}p < 0.01$ vs. 0 μM).

Western blot analysis demonstrated that 312 μM BUP significantly decreased BCL2 expression and increased BAX expression, resulting in an elevated BAX/BCL2 ratio (Fig. 5B, C; $^{*}p < 0.05$ to $^{**}p < 0.01$ vs. 0 μM). Cytochrome c (CYTO-C) release was significantly upregulated, and cleaved caspase-3 (A-CASPASE3) levels were markedly increased in BUP-treated cells compared with controls (Fig. 5B, C; $^{*}p < 0.05$ to $^{**}p < 0.01$). These findings demonstrate that BUP induces intracellular oxidative stress and activates the mitochondrial apoptotic pathway, as evidenced by cytochrome c protein and caspase-3 cleavage, raising the question of whether these effects can be pharmacologically attenuated by lipid emulsion rescue therapy.

3.6 Lipid emulsion attenuates bupivacaine-induced mitochondrial dysfunction, oxidative stress, and apoptosis

To evaluate the protective effect of lipid emulsion (LE) against BUP-induced cardiotoxicity, hiPSC-CMs were co-treated with 312 μM BUP and LE at concentrations of 0, 1, or 2% for 24 h (Fig. 6). LE alone (0–2%) did not significantly affect cell viability at any concentration tested, confirming its safety profile at the doses used (Fig. 6A). Co-treatment with LE at 1% and 2% significantly restored cell viability in BUP-treated cells compared with the BUP-alone group (Fig. 6B; $^{**}p < 0.01$ for LE 1%, $^{*}p < 0.05$ for LE 2% vs. LE 0%).

JC-1 staining demonstrated that LE co-treatment partially restored the J-aggregates/J-monomers ratio in BUP-treated cells, with significant recovery observed at both 1% and 2% LE (Fig. 6C; $^{**}p < 0.01$ and $^{*}p < 0.05$, respectively). Intracellular ROS levels were significantly reduced by LE co-treatment compared with the BUP-alone group (Fig. 6D; $^{*}p < 0.05$ vs. LE 0%). Western blot analysis showed that co-treatment with 1% LE significantly increased BCL2 expression, decreased BAX and CYTO-C levels, and reduced cleaved caspase-3 compared with BUP-treated controls (Fig. 6E, F; $^{*}p < 0.05$ vs. LE 1% + BUP 0 μM). Furthermore, LE co-treatment significantly decreased DRP1 expression and increased OPA1 expression, suggesting partial restoration of mitochondrial fusion–fission balance (Fig. 6G, H; $^{*}p < 0.05$ vs. LE 1% + BUP 0 μM). These findings suggest that Intralipid partially reverses bupivacaine-induced mitochondrial

dysfunction and apoptosis in hiPSC-CMs, providing a mechanistic basis for its clinical use as a rescue agent in bupivacaine-induced cardiac toxicity.

4 Discussions

Core Findings in Context of Existing Literature

The present study demonstrates that bupivacaine induces dose- and time-dependent cytotoxicity in hiPSC-CMs, with IC_{50} values of 550 μM at 24 h and 312 μM at 48 h, and that this toxicity is mechanistically linked to mitochondrial dysfunction, oxidative stress, and activation of the intrinsic apoptotic pathway. These findings are broadly consistent with prior reports of bupivacaine-induced cardiotoxicity across multiple experimental models. Sztark et al. first demonstrated that bupivacaine directly inhibits mitochondrial complex I activity in isolated rat cardiac mitochondria, resulting in impaired oxidative phosphorylation and reduced ATP synthesis at clinically relevant concentrations (Sztark et al. 1998). Yang et al. demonstrated bupivacaine-induced mitochondrial fragmentation and caspase-3 activation in H9c2 cardiomyoblasts, corroborating our observations in a human pluripotent stem cell-derived model (Yang et al. 2015). Importantly, the present study extends these findings by employing hiPSC-CMs, a genetically human, patient-relevant cardiac model, thereby bridging the translational gap between rodent-based mechanistic studies and human cardiac physiology. The spontaneous beating impairment observed at 312–550 μM further adds a functional electromechanical dimension that is not captured by conventional cytotoxicity assays alone, reinforcing the utility of hiPSC-CMs as a platform for cardiotoxicity assessment.

Mechanistic Interpretation: The Mitochondria–ROS–Apoptosis Axis

The mechanistic data presented here support a coherent pathological cascade in which bupivacaine-induced mitochondrial injury serves as the proximal event driving downstream oxidative stress and apoptotic cell death. Bupivacaine suppresses the activity of mitochondrial respiratory chain complexes — particularly complex I and complex IV — leading to collapse of the mitochondrial membrane potential (ΔΨm) and impaired ATP production in cardiomyocytes (Lv et al. 2016; Chen et al. 2017). Our JC-1 data directly confirm ΔΨm depolarization at 312 and 550 μM, consistent with this mechanism. The concurrent shift in mitochondrial dynamics, characterized by downregulation of fusion mediators MFN1, MFN2, and OPA1, and upregulation of fission effectors DRP1 and FIS1, is mechanistically significant. Mitochondrial fission is now recognized not merely as a morphological response but as an active amplifier of apoptotic signaling: DRP1-mediated fragmentation facilitates BAX oligomerization at the outer mitochondrial membrane, promoting cytochrome c release into the cytosol (Youle and van der Bliek 2012). The elevated intracellular ROS levels observed in our DCFH-DA assay are consistent with impaired complex I activity generating superoxide at the flavin mononucleotide site, a well-characterized consequence of electron transport chain inhibition (Murphy 2009). Collectively, the sequential activation of ΔΨm collapse → DRP1-driven fission → cytochrome c release → caspase-3 cleavage observed in our data constitutes an intrinsic apoptotic cascade, and our findings provide the first direct evidence of this complete

pathway in a human iPSC-derived cardiac model exposed to bupivacaine. This mechanistic clarity has direct implications for therapeutic targeting, as each node in this cascade represents a potential intervention point.

Lipid Emulsion Rescue: Lipid Sink, Energetic Support, and Clinical Relevance

The observation that co-treatment with Intralipid (1–2%) significantly attenuated bupivacaine-induced cytotoxicity, mitochondrial depolarization, oxidative stress, and apoptotic signaling provides important mechanistic support for the clinical use of lipid emulsion in local anesthetic systemic toxicity (LAST). The American Society of Regional Anesthesia and Pain Medicine (ASRA) currently recommends intravenous lipid emulsion (ILE) as a first-line adjunct in the management of LAST, particularly in cases of cardiovascular collapse refractory to standard resuscitation (Nendumba et al. 2025). Two principal mechanisms have been proposed to explain ILE efficacy. The lipid sink hypothesis posits that the exogenous lipid phase creates a pharmacokinetic reservoir that sequesters free bupivacaine from cardiac tissue, reducing its effective intracellular concentration (Neal et al. 2018). The direct metabolic support hypothesis, alternatively, proposes that fatty acids liberated from the lipid emulsion serve as preferred oxidative substrates for the energy-depleted myocardium, partially restoring mitochondrial ATP production independent of drug sequestration (Fettiplace and Weinberg 2018). Our data provide evidence consistent with both mechanisms: the restoration of $\Delta\Psi m$ and reduction in DRP1/FIS1 expression suggest improved mitochondrial energetics, while the concurrent reduction in intracellular bupivacaine-mediated ROS generation is consistent with reduced drug bioavailability at the mitochondrial membrane. Notably, the partial — rather than complete — rescue of mitochondrial fusion–fission balance and apoptotic markers by ILE in our model suggests that neither mechanism alone is sufficient, and that the clinical efficacy of ILE likely reflects a composite effect. These findings reinforce the mechanistic rationale for the ASRA LAST guidelines and suggest that optimizing lipid emulsion dosing to maximize both sequestration and metabolic support warrants further investigation in human cardiac models.

Limitations and Future Directions

Several limitations of the present study should be acknowledged. First, the use of a single hiPSC line from one healthy donor ensures experimental consistency but limits generalizability across individuals with diverse genetic backgrounds or pharmacogenomic profiles. Future studies employing patient-specific or isogenic hiPSC lines will be valuable in characterizing inter-individual variability in bupivacaine sensitivity. Second, the static in vitro exposure model does not fully recapitulate bupivacaine pharmacokinetics in vivo. Given that bupivacaine is approximately 95% plasma protein-bound, the free drug concentrations applied here represent an upper-bound exposure scenario directly relevant to accidental intravascular injection, the clinical context most pertinent to LAST. Validation in dynamic perfusion systems and in vivo models remains an important next step.

Conclusions

This study shows that bupivacaine induces dose- and time-dependent cardiotoxicity in hiPSC-CMs, accompanied by mitochondrial membrane depolarization, dysregulated mitochondrial dynamics, increased oxidative stress, and activation of intrinsic apoptotic signaling. Intralipid co-treatment partially attenuated these effects by preserving mitochondrial membrane potential, reducing ROS accumulation, and suppressing apoptosis-associated protein changes. These findings provide human cardiac cell-based evidence supporting a mitochondria–ROS–apoptosis mechanism in bupivacaine-induced cardiotoxicity and offer mechanistic support for lipid emulsion therapy in LAST-associated cardiac injury.

Declarations

Author contributions

T.J. and Z.Z. contributed equally to this work. T.J., Z.Z., and Y.M. conceived and designed the study. T.J. and Z.Z. performed the majority of the experiments, including hiPSC-CM differentiation and culture, bupivacaine and Intralipid treatment, cell viability assays, and data analysis. W.H. and M.W. assisted with the assessment of mitochondrial membrane potential, reactive oxygen species, and mitochondrial morphology. N.W. and W.S. performed Western blotting and apoptosis assays. S.Z. contributed to the statistical analysis and data interpretation. T.J. and Z.Z. wrote the main manuscript text. Y.M. supervised the project, acquired funding and resources, and critically revised the manuscript. All authors reviewed and approved the final manuscript.

Data Availability Statement

The data that support the findings of this study are available from the corresponding author upon reasonable request.

Conflicts of Interest

The authors report no conflicts of interest in this work.

Funding

This work was supported, by the Natural Science Foundation of Xi’an Health Commission [no. 2025qn11],and the Natural Science Foundation of Xi’an Children’s Hospital [no. 2024I01].

Ethics Statement

Not applicable.

References

1. El-Boghdadly K, Pawa A, Chin KJ (2018) Local anesthetic systemic toxicity: current perspectives [J]. Local Reg Anesth 11:35–44

2. El-Boghdadly K, Chin KJ (2016) Local anesthetic systemic toxicity: continuing professional development [J]. Can J Anaesth 63(3):330–349
3. Marrone F, Sbucafratta L, Fusco P (2026) The fascial plane blocks in the upper arm surgery and trauma: a narrative review [J]. J Clin Anesth 109:112115
4. Neal JM, Woodward CM, Harrison TK (2018) The American Society of Regional Anesthesia and Pain Medicine checklist for managing local anesthetic systemic toxicity: 2017 version [J]. Reg Anesth Pain Med 43(2):150–153
5. Sztark F, Malgat M, Dabadie P et al (1998) Comparison of the effects of bupivacaine and ropivacaine on heart cell mitochondrial bioenergetics [J]. Anesthesiology 88(5):1340–1349
6. Lu J, Xu SY, Zhang QG et al (2011) Bupivacaine induces apoptosis via mitochondria and p38 MAPK dependent pathways [J]. Eur J Pharmacol 657(1–3):51–58
7. Haraguchi Y, Ohtsuki A, Oka T et al (2015) Electrophysiological analysis of mammalian cells expressing hERG using automated 384-well-patch-clamp [J]. BMC Pharmacol Toxicol 16:39
8. Karakikes I, Ameen M, Termglinchan V et al (2015) Human induced pluripotent stem cell-derived cardiomyocytes: insights into molecular, cellular, and functional phenotypes [J]. Circ Res 117(1):80–88
9. Ewoldt JK, DePalma SJ, Jewett ME et al (2025) Induced pluripotent stem cell-derived cardiomyocyte in vitro models: benchmarking progress and ongoing challenges [J]. Nat Methods 22(1):24–40
10. Nendumba G, Blackman S, De Lissnyder N et al (2025) Use of intravenous lipid emulsions in drug-induced toxicities: a 2025 narrative review [J]. Ann Intensive Care 15(1):181
11. Lian X, Zhang J, Azarin SM et al (2013) Directed cardiomyocyte differentiation from human pluripotent stem cells by modulating Wnt/β-catenin signaling under fully defined conditions [J]. Nat Protoc 8(1):162–175
12. Yang L, Bai Z, Lv D et al (2015) Rescue effect of lipid emulsion on bupivacaine-induced cardiac toxicity in cardiomyocytes [J]. Mol Med Rep 12(3):3739–3747
13. Lv D, Bai Z, Yang L et al (2016) Lipid emulsion reverses bupivacaine-induced apoptosis of h9c2 cardiomyocytes: PI3K/Akt/GSK-3β signaling pathway [J]. Environ Toxicol Pharmacol 42:85–91
14. Chen Z, Jin Z, Xia Y et al (2017) The protective effect of lipid emulsion in preventing bupivacaine-induced mitochondrial injury and apoptosis of H9C2 cardiomyocytes [J]. Drug Deliv 24(1):430–436
15. Youle RJ, van der Bliek AM (2012) Mitochondrial fission, fusion, and stress [J]. Science 337(6098):1062–1065
16. Murphy MP (2009) How mitochondria produce reactive oxygen species [J]. Biochem J 417(1):1–13
17. Neal JM, Barrington MJ, Fettiplace MR et al (2018) The third American Society of Regional Anesthesia and Pain Medicine practice advisory on local anesthetic systemic toxicity: executive summary 2017 [J]. Reg Anesth Pain Med 43(2):113–123
18. Fettiplace MR, Weinberg G (2018) The mechanisms underlying lipid resuscitation therapy [J]. Reg Anesth Pain Med 43(2):138–149

Figures

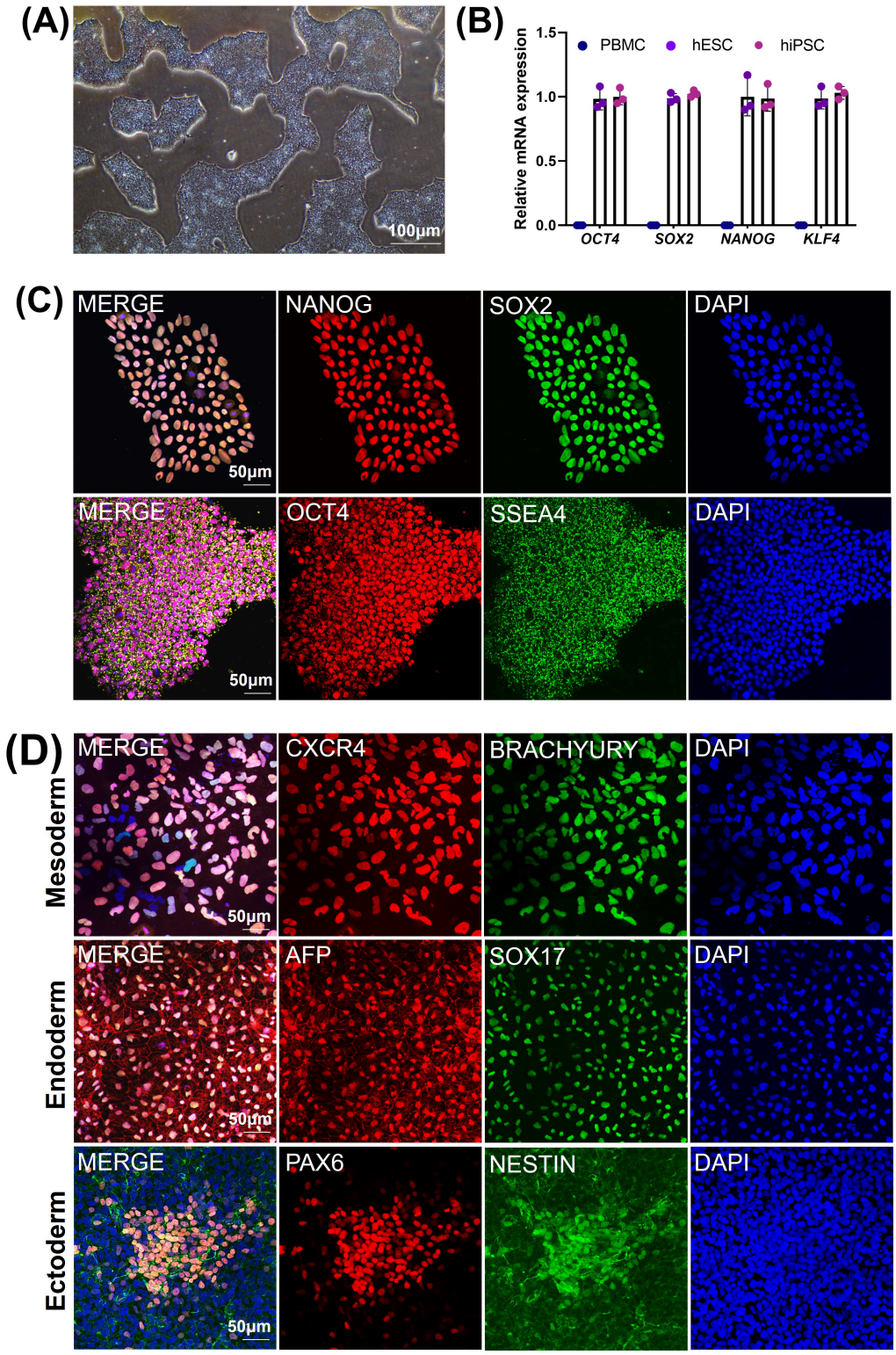


Figure 1

Characterization of hiPSC. (A) Representative bright-field image showing the typical colony morphology of hiPSC. Scale bar, 100 μm. (B) qRT-PCR analysis of pluripotency marker genes (OCT4, SOX2, NANOG, and KLF4) in PBMC, hESC, and hiPSC. Expression values were normalized to GAPDH. Data are presented

as mean ± SD; n = 3. (C) Immunofluorescence staining of pluripotency markers in hiPSC colonies. Nuclear markers NANOG (red) and SOX2 (green) are shown in the upper panel; OCT4 (red) and surface marker SSEA4 (green) are shown in the lower panel. Nuclei were counterstained with DAPI (blue). Scale bar, 50 μm. (D) Immunofluorescence analysis of three-germ-layer differentiation capacity. Upper panel: mesoderm markers CXCR4 (red) and BRACHYURY (green); middle panel: endoderm markers AFP (red) and SOX17 (green); lower panel: ectoderm markers PAX6 (red) and NESTIN (green). Nuclei were counterstained with DAPI (blue). Scale bar, 50 μm.

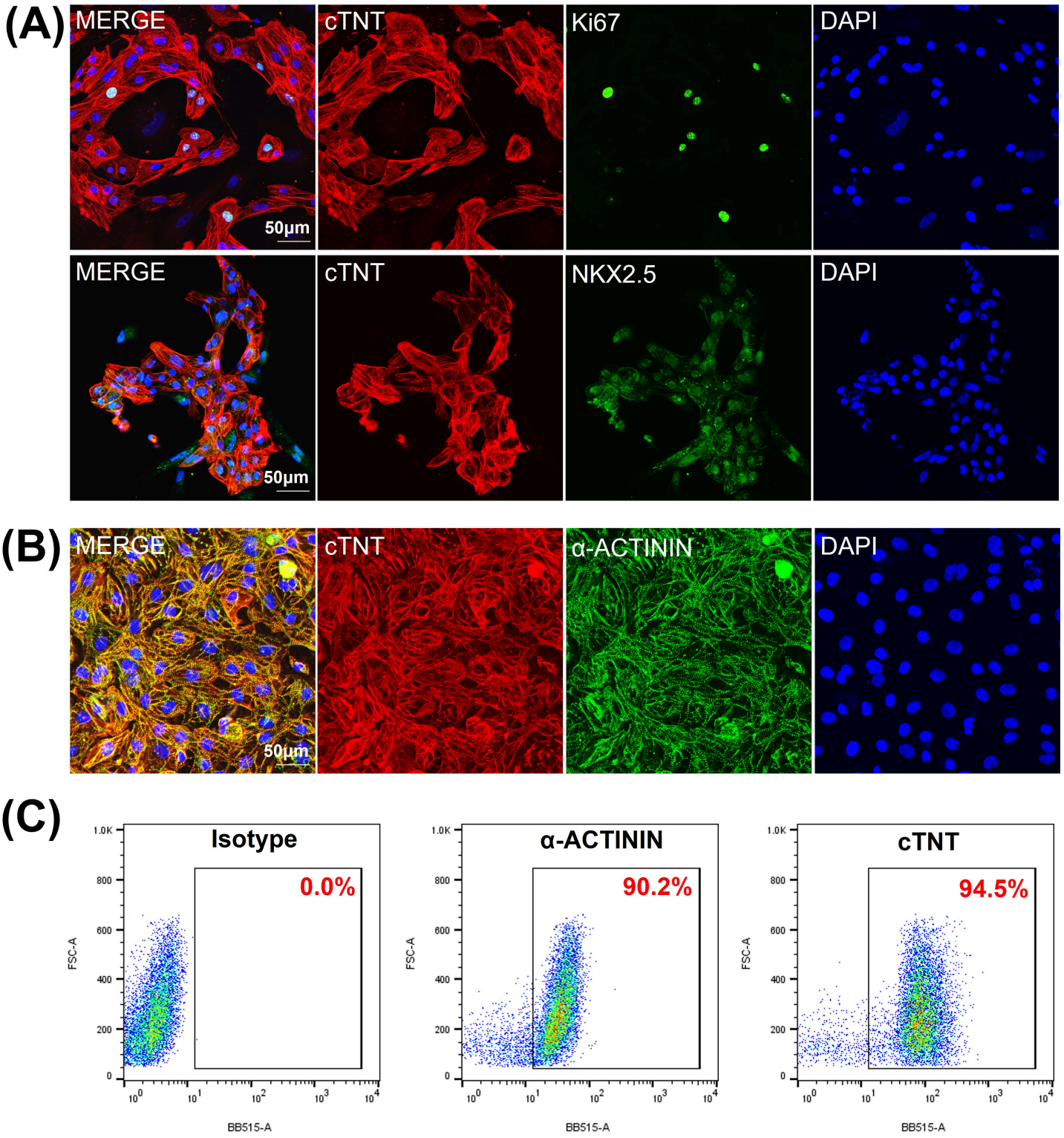


Figure 2

Characterization of hiPSC-derived cardiomyocytes. (A) Immunofluorescence staining of hiPSC-derived cardiomyocytes at day 21. Upper panel: cTNT (red) and proliferation marker Ki67 (green); lower panel: cTNT (red) and cardiac progenitor marker NKX2.5 (green). Nuclei were counterstained with DAPI (blue). Scale bar, 50 μm. (B) Immunofluorescence staining of hiPSC-derived cardiomyocytes at day 35, showing sarcomeric proteins cTNT (red) and α-actinin (green) with well-organized myofibrillar structures indicative of increased maturation. Nuclei were counterstained with DAPI (blue). Scale bar, 50 μm. (C) Flow cytometry analysis of cardiomyocyte purity at day 21. Representative scatter plots show 90.2% α-actinin-positive and 94.5% cTNT-positive cells, with an unstained blank as negative control.

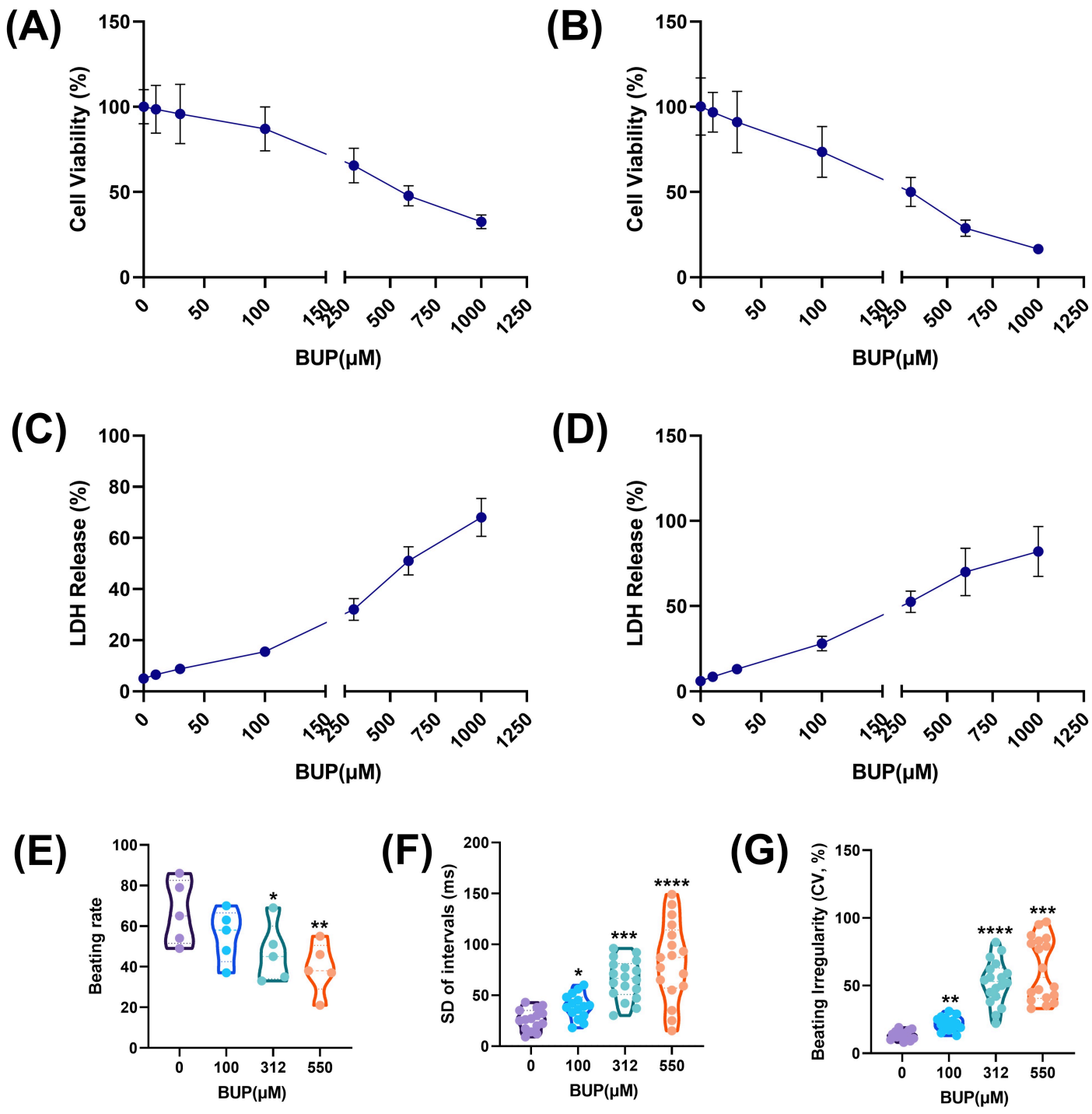


Figure 3

Dose-dependent cytotoxicity and functional impairment of bupivacaine in hiPSC-derived cardiomyocytes. (A, B) Cell viability assessed by CCK-8 assay following exposure to bupivacaine (0–1000 μM) for 24 h (A) and 48 h (B). Data are presented as mean ± SD; n = 5. (C, D) LDH release as an index of membrane integrity following bupivacaine exposure for 24 h (C) and 48 h (D). Data are presented as mean ± SD; n = 5. (E) Spontaneous beating rate of hiPSC-derived cardiomyocytes following 24 h bupivacaine treatment (0, 100, 312, and 550 μM). Data are presented as violin plots; n = 5. (F) Standard deviation of inter-beat intervals following 24 h bupivacaine treatment. Data are presented as

violin plots; n = 15, 15, 18, and 16 for 0, 100, 312, and 550 μM groups, respectively. (G) Beating irregularity expressed as coefficient of variation (CV, %) following 24 h bupivacaine treatment. Data are presented as violin plots; n = 15, 15, 18, and 18 for 0, 100, 312, and 550 μM groups, respectively. One-way ANOVA with post hoc test; *p < 0.05, **p < 0.01, ***p < 0.001, ****p < 0.0001 vs. 0 μM.

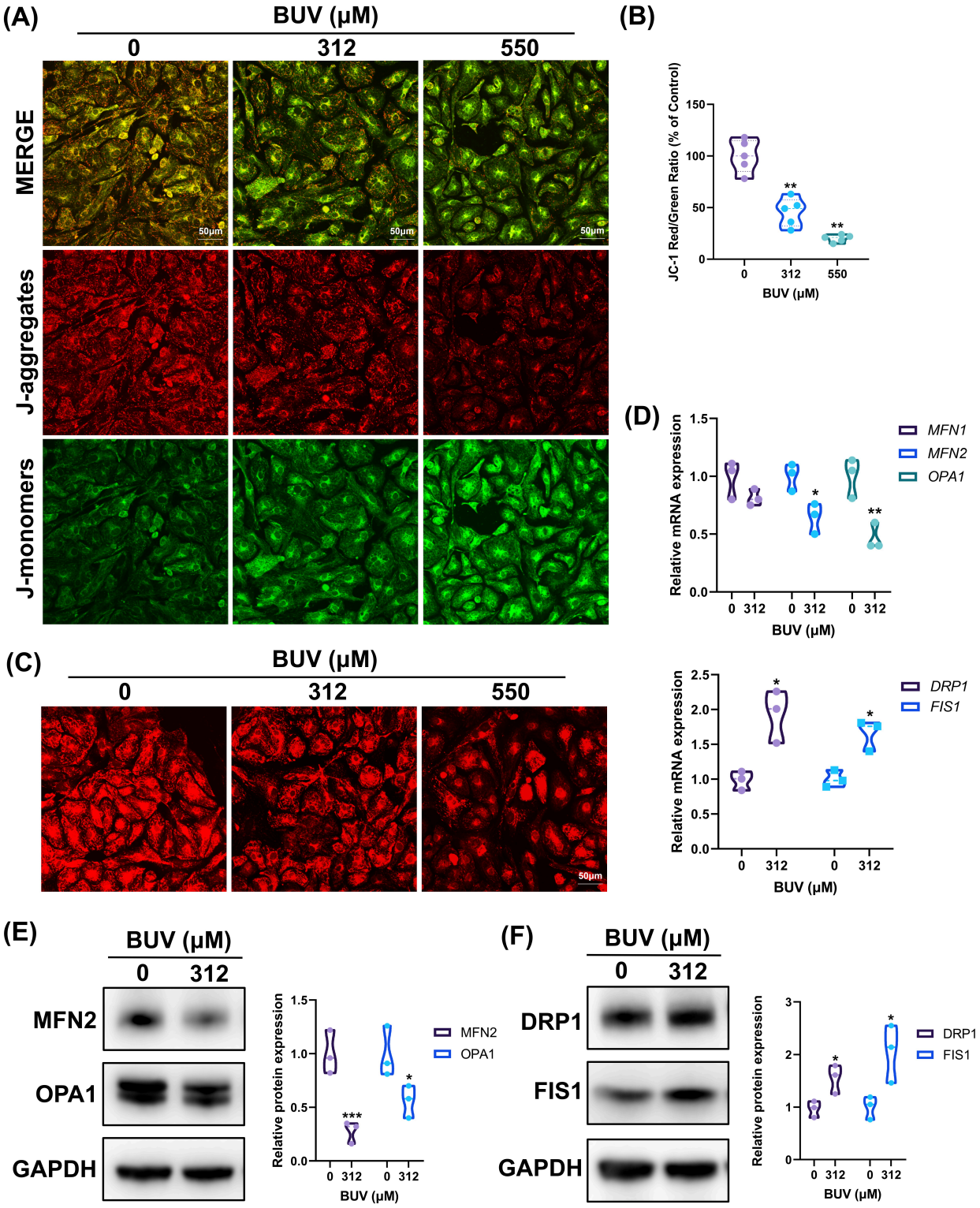


Figure 4

Bupivacaine induces mitochondrial damage in hiPSC-derived cardiomyocytes. (A) Representative JC-1 fluorescence images of hiPSC-derived cardiomyocytes treated with bupivacaine (0, 312, and 550 μM) for 24 h. J-aggregates (red, high mitochondrial membrane potential) and J-monomers (green, low mitochondrial membrane potential) are shown separately and as merged images. Scale bars, 50 μm. (B) Quantification of the J-aggregates/J-monomers fluorescence intensity ratio. Data are presented as violin plots; n = 5. One-way ANOVA with post hoc test; **p < 0.01 vs. 0 μM. (C) Representative MitoTracker Red fluorescence images showing mitochondrial morphology in hiPSC-derived cardiomyocytes treated with bupivacaine (0, 312, and 550 μM) for 24 h. Progressive mitochondrial fragmentation is observed with increasing concentrations. Scale bar, 50 μm. (D) Relative mRNA expression of mitochondrial fusion genes (MFN1, MFN2, and OPA1; upper panel) and fission genes (DRP1 and FIS1; lower panel) in hiPSC-derived cardiomyocytes treated with bupivacaine (0 or 312 μM) for 24 h. Expression was normalized to GAPDH. Data are presented as violin plots; n = 3. Unpaired t-test; *p < 0.05, **p < 0.01 vs. 0 μM. (E) Representative Western blot images and quantification of fusion-related proteins MFN2 and OPA1 in hiPSC-derived cardiomyocytes treated with bupivacaine (0 or 312 μM) for 24 h. GAPDH served as the loading control. Data are presented as violin plots; n = 3. Unpaired t-test; *p < 0.05, ***p < 0.001 vs. 0 μM. (F) Representative Western blot images and quantification of fission-related proteins DRP1 and FIS1 in hiPSC-derived cardiomyocytes treated with bupivacaine (0 or 312 μM) for 24 h. GAPDH served as the loading control. Data are presented as violin plots; n = 3. Unpaired t-test; *p < 0.05 vs. 0 μM.

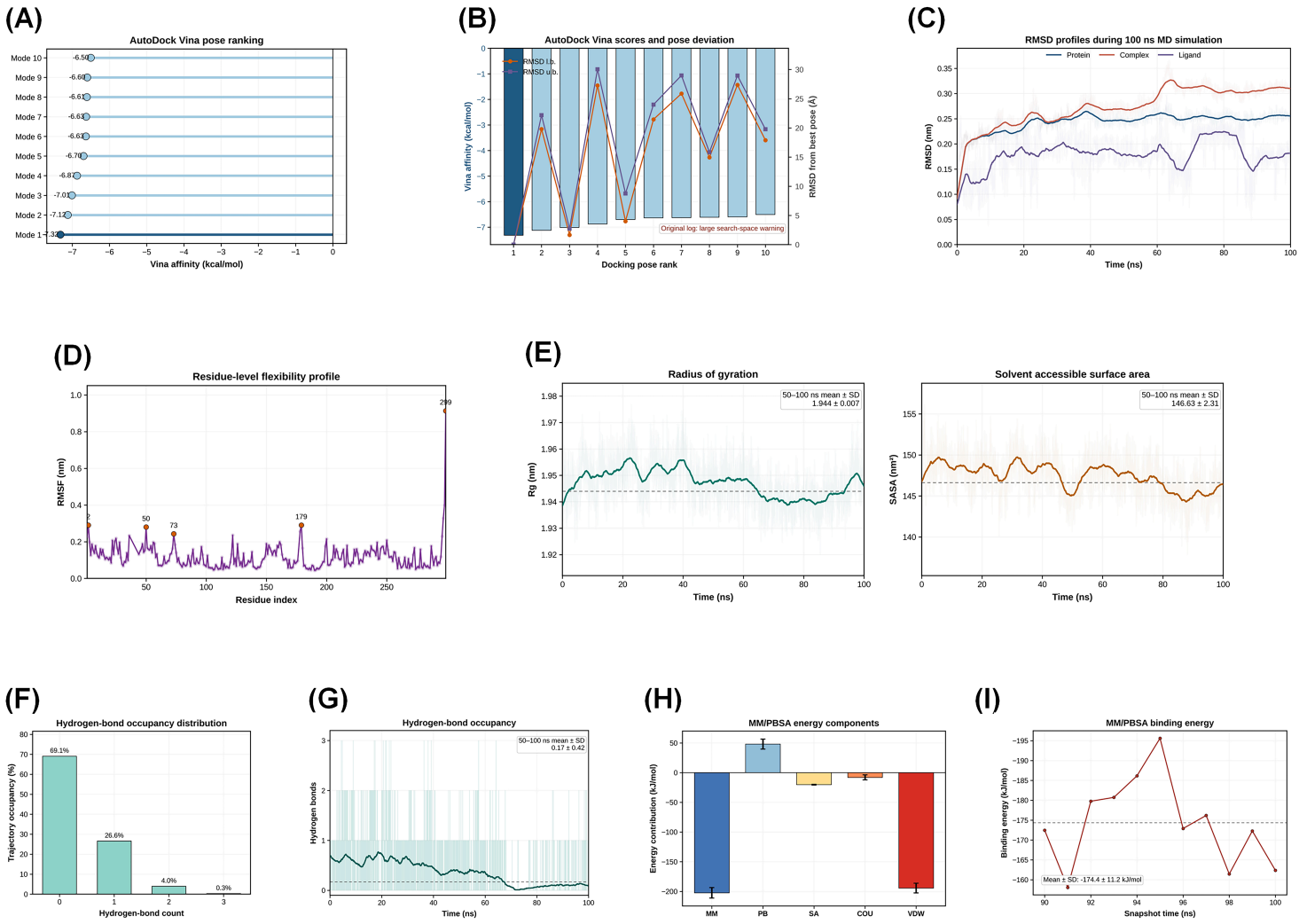


Figure 5

Bupivacaine induces oxidative stress and activates the mitochondrial apoptotic pathway in hiPSC-derived cardiomyocytes. (A) Intracellular ROS levels in hiPSC-derived cardiomyocytes treated with bupivacaine (0, 312, and 550 μM) for 24 h, expressed as percentage relative to the 0 μM group. Data are presented as violin plots; n = 5. One-way ANOVA with post hoc test; **p < 0.01 vs. 0 μM. (B) Representative Western blot images of BCL2, BAX, cytochrome c (CYTO-C), and cleaved caspase-3 (A-CASPASE3) in hiPSC-derived cardiomyocytes treated with bupivacaine (0 or 312 μM) for 24 h. GAPDH served as the loading control. (C) Quantification of relative protein expression levels of BCL2, BAX, CYTO-C, and A-CASPASE3. Data are presented as violin plots; n = 3. Unpaired t-test; *p < 0.05, **p < 0.01 vs. 0 μM.

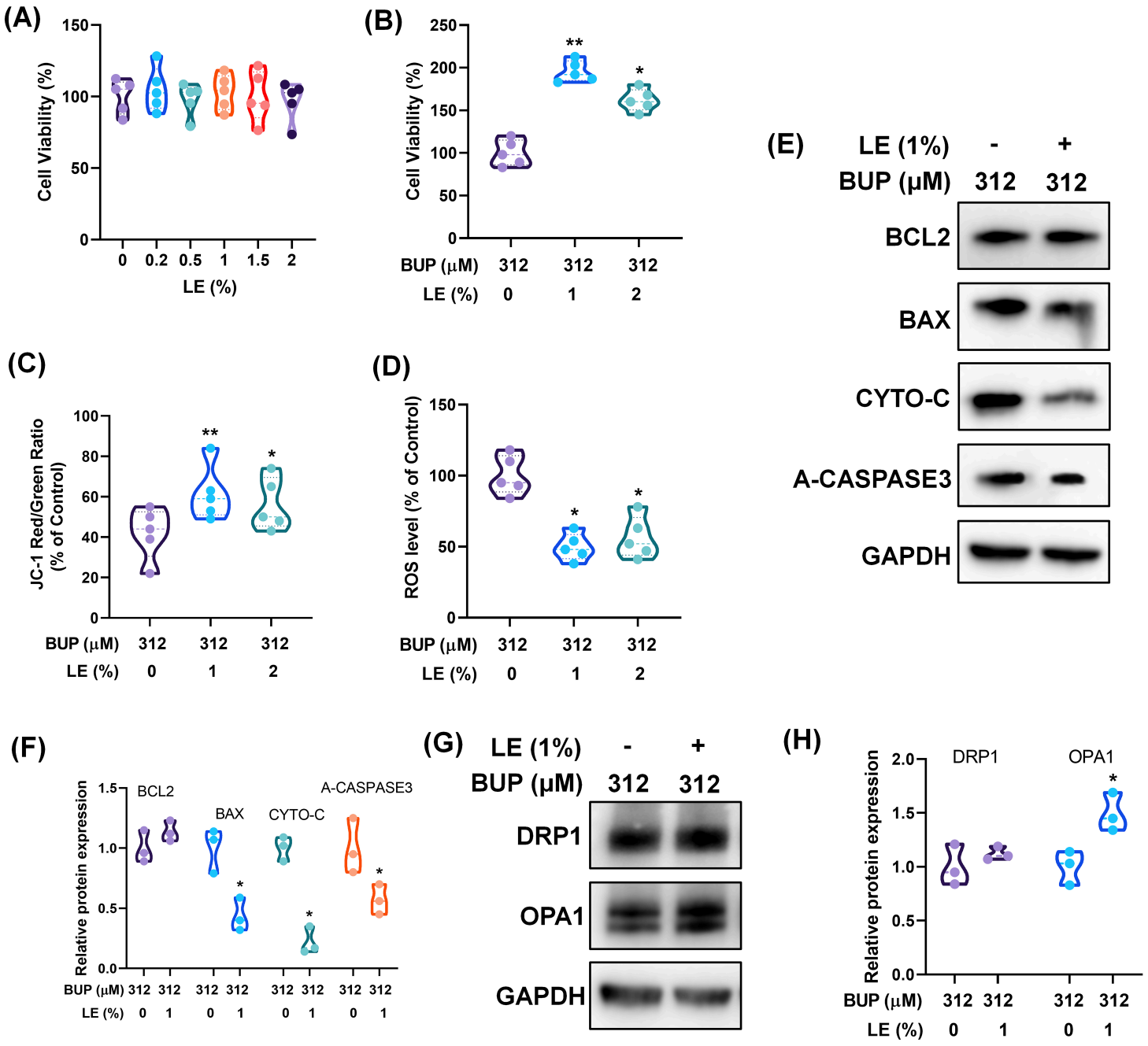


Figure 6

Lipid emulsion attenuates bupivacaine-induced mitochondrial dysfunction, oxidative stress, and apoptosis in hiPSC-derived cardiomyocytes. (A) Cell viability of hiPSC-derived cardiomyocytes treated with increasing concentrations of lipid emulsion (LE; 0, 0.2, 0.5, 1, 1.5, and 2%) for 24 h, assessed by CCK-8 assay. Data are presented as violin plots; n = 5. One-way ANOVA with post hoc test; no significant difference was observed across groups. (B) Cell viability of hiPSC-derived cardiomyocytes co-treated with bupivacaine (312 μM) and LE (0, 1, or 2%) for 24 h. Data are presented as violin plots; n = 5. One-way ANOVA with post hoc test; **p < 0.01 (LE 1% vs. LE 0%), *p < 0.05 (LE 2% vs. LE 0%). (C) JC-1 Red/Green fluorescence ratio in hiPSC-derived cardiomyocytes co-treated with bupivacaine (312 μM) and LE (0, 1, or 2%), expressed as percentage of the untreated control. Data are presented as violin plots; n = 5. One-way

ANOVA with post hoc test; **p < 0.01 (LE 1% vs. LE 0%), *p < 0.05 (LE 2% vs. LE 0%). (D) Intracellular ROS levels in hiPSC-derived cardiomyocytes co-treated with bupivacaine (312 μM) and LE (0, 1, or 2%), expressed as percentage of the untreated control. Data are presented as violin plots; n = 5. One-way ANOVA with post hoc test; *p < 0.05 vs. LE 0%. (E) Representative Western blot images of BCL2, BAX, cytochrome c (CYTO-C), and cleaved caspase-3 (A-CASPASE3) in hiPSC-derived cardiomyocytes co-treated with LE (1%) and bupivacaine (0 or 312 μM). GAPDH served as the loading control. (F) Quantification of relative protein expression levels of BCL2, BAX, CYTO-C, and A-CASPASE3. Data are presented as violin plots; n = 5. Unpaired t-test; *p < 0.05 vs. LE 1% + BUP 0 μM. (G) Representative Western blot images of DRP1 and OPA1 in hiPSC-derived cardiomyocytes co-treated with LE (1%) and bupivacaine (0 or 312 μM). GAPDH served as the loading control. (H) Quantification of relative protein expression levels of DRP1 and OPA1. Data are presented as violin plots; n = 5. Unpaired t-test; *p < 0.05 vs. LE 1% + BUP 0 μM.

Supplementary Files

This is a list of supplementary files associated with this preprint. Click to download.

- TableS1.docx